

Spin interaction and magnetism in cobaltate Kitaev candidate materials: an *ab initio* and model Hamiltonian approach

Shishir Kumar Pandey¹ and Ji Feng^{1, 2, 3, *}

¹*International Center for Quantum Materials, School of Physics, Peking University, Beijing 100871, China*

²*Collaborative Innovation Center of Quantum Matter, Beijing 100871, China*

³*CAS Center for Excellence in Topological Quantum Computation,
University of Chinese Academy of Sciences, Beijing 100190, China*

(Dated: May 10, 2022)

In the quest for materials hosting Kitaev spin liquids, much of the efforts have been focused on the fourth- and fifth-row transition metal compounds, which are spin-orbit coupling assisted Mott insulators. Here, we study the structural and magnetic properties of 3d transition metal oxides, Na₂Co₂TeO₆ and Na₃Co₂SbO₆. The partial occupancy of sodium in former compound is addressed using a cluster expansion, and a honeycomb lattice of sodiums is found to be energetically favored. Starting from the *ab initio* band structures, a many-body second order perturbation theory leads to a pseudospin- $\frac{1}{2}$ Hamiltonian with estimated magnetic interactions. We show that the experimentally observed zigzag magnetic state is stabilised only when the first neighbour Kitaev coupling dominates over the Heisenberg term, both of which are highly suppressed due to presence of e_g orbitals. A third neighbour Heisenberg interaction is found dominant in both these compounds. We also present a phase diagram for Na₂Co₂TeO₆ by varying Hubbard- U and spin-orbit coupling- λ . Spin excitation spectra are found to capture essential features of recent experimental magnon spectrum, lending support to our results.

I. Introduction

Strong quantum fluctuations in the ground state of a many-spin system can produce a quantum spin liquid state, in which spins are highly entangled even at large separations without any long-range order [1, 2]. Realisation of quantum spin liquid in actual materials is clearly attractive, especially for its potential application in quantum computation [3], and high- T_c superconductivity [4]. Known candidate materials that may host a spin liquid state are few [5–8], and the quest for new potential candidates has recently drawn a lot of attention triggered by the pioneering work of Kitaev who proposed an exactly solvable spin model on triply coordinated lattice, exhibiting degenerate spin-liquid ground states [3]. Extension of the Kitaev’s honeycomb lattice model [9] to the inclusion of bond-dependent, highly anisotropic Heisenberg coupling interactions inherently introduces frustration to the spin system, and may be conducive to the realisation of quantum spin liquid states.

A host of transition-metal compounds have been proposed as a material candidates for realising the Kitaev physics [10–24]. Nevertheless, compounds containing a 3d element distinguishes themselves from 4/5d compounds. On one hand, crystal fields (CF) and spin-orbit coupling (SOC) are believed to be substantially stronger in 4/5d compounds than in their third-row counterparts. On the other hand, 3d elements are considerably more compact and the localisation of d orbitals results in larger Hubbard U and intra-atomic Hund’s coupling compared to 4/5d compounds. Much of previous attention has

been paid to 4/5d magnetic materials, in which the interplay of Hubbard interaction (U), intra-atomic Hund’s exchange (J_h), CF (Δ) and the SOC (λ) leads to intricate Mott insulating states [25–37]. The studies focusing 3d material are few and limited mostly to theoretical models [10, 11, 13]. A quantitative examination based on *ab initio* electronic structure methods of the electronic and magnetic structure of the co-based compounds, Na₂Co₂TeO₆ and Na₃Co₂SbO₆, is evidently in order.

Each Co⁺² with seven d electrons in a nearly octahedral CF of oxygens in these materials shows a high-spin $t_{2g}^5 e_g^2$ configuration. The d electrons on an isolated Co ion is then described by an effective spin $S = 3/2$ and orbital angular momentum $L = 1$, giving rise to a low-energy pseudospin-1/2 doublet after application of SOC. Similar to iridates and RuCl₃, experiments propose zigzag magnetic ground state also for Na₂Co₂TeO₆ and Na₃Co₂SbO₆ [38–40]. What makes these d^7 cobaltates more interesting material to study when compared to those of d^5 iridates or RuCl₃ is the additional presence of spin-only active e_g orbitals.

In transition metal compounds, origin of anisotropic magnetic interactions such as Kitaev interaction is attributed to the directional nature of transition metal d orbitals. Interaction of unquenched orbital moments with spin moments in such materials via spin-orbit interaction (SOI) may give rise to such type of non-trivial anisotropic exchange coupling. Under large CF present in 4/5d compounds, low energy space of d^5 configuration of transition metal ions in these materials can be described by a single hole with effective spin moment (\mathbf{S}) = 1/2 and effective orbital angular momentum (\mathbf{L}) = 1 within the t_{2g} manifold. SOC then leads to an effective total angular momentum of $\mathbf{J}_{\text{eff}} = \mathbf{S} - \mathbf{L}$ forming doubly degenerate pseudospins

* jfeng11@pku.edu.cn

-1/2 ground state.

Based on above discussion, several interesting questions arises about structural, electronic and magnetic properties of cobaltates. Like for example, at the magnetic front, questions like whether cobaltates are a Kitaev-type material, if yes, is it in a close proximity to quantum spin liquid state, would be interesting to answer. About structural property, questions like how to deal with the partial occupancy of Na sites and whether it can influence the electronic or the magnetic properties of $\text{Na}_2\text{Co}_2\text{TeO}_6$ compound would be important to answer. In present study, we first attempt to fix the issue of partial occupancy of Na sites. We employ a Cluster-expansion method with which we obtain particular pattern formation of Na atoms in the supercell of $\text{Na}_2\text{Co}_2\text{TeO}_6$. In the next step, using second order perturbation method, we evaluate the magnetic interactions between the Co^{+2} ions in terms of pseudospins-1/2 for both $\text{Na}_2\text{Co}_2\text{TeO}_6$ and $\text{Na}_3\text{Co}_2\text{SbO}_6$. Hopping amplitudes and CF splitting were estimated from a Wannier based tight binding (TB) approach. We show that Heisenberg interactions as well as off-diagonal couplings are all highly suppressed and the dominant interaction is Kitaev-type for first nearest neighbour (1NN) Co atoms. Trigonal CF splitting, although comparable to the strength of SOC in these materials, it does not alter the pseudospin-1/2 picture. The second nearest neighbour (2NN) and inter-layer magnetic interactions were found to be either negligibly small or identically zero. Contrary to $4d/5d$ based Kitaev-materials, quite surprisingly, the third nearest neighbor (3NN) magnetic interactions are significantly larger than the 1NN ones. A suppressed Kitaev coupling and appearance of off-diagonal terms were found for 3NNs. Spin-wave spectra obtained using these magnetic interactions in a Heisenberg-Kitaev model shows qualitative agreement with experiments. By varying parameters Hubbard U and SOC strength- λ we obtain a phase diagram for $\text{Na}_2\text{Co}_2\text{TeO}_6$. We find different type of zigzag magnetic ordering stabilised in major portion of the phase diagram. We extensively discuss the properties of $\text{Na}_2\text{Co}_2\text{TeO}_6$ in this study and finish our discussion in the end with a brief comparison between the properties of $\text{Na}_2\text{Co}_2\text{TeO}_6$ and $\text{Na}_3\text{Co}_2\text{SbO}_6$.

II. $\text{Na}_2\text{Co}_2\text{TeO}_6$

A. Structure and Na vacancies

In this section, we present the results concerning the basic structure and electronic structure of $\text{Na}_2\text{Co}_2\text{TeO}_6$ obtained from *ab initio* calculations. We will discuss properties of $\text{Na}_3\text{Co}_2\text{SbO}_6$ later in Sec. III. The issue of Na partial occupancy in $\text{Na}_2\text{Co}_2\text{TeO}_6$ is resolved using a cluster-expansion model to aid a global survey of the energy landscape of the vacancy disorder, which suggests that the vacancy is likely to be ordered in-plane and there is a stacking disorder of Na layers.

Before proceeding to the discussions of the crystal and basic electronic structures, let us briefly describe the computational details of the *ab initio* calculations. To calculate the total energies and electronic structure of $\text{Na}_2\text{Co}_2\text{TeO}_6$, we perform density functional theory calculations within the generalised-gradient approximation (GGA). [41] Planewave basis set with a cutoff at 550 eV with projected augmented wave potentials [42–44] is used, with a $8 \times 8 \times 4/6 \times 3 \times 6$ k -grid for the Brillouin zone sum for calculations on the primitive cell of $\text{Na}_2\text{Co}_2\text{TeO}_6/\text{Na}_3\text{Co}_2\text{SbO}_6$, and a $6 \times 6 \times 3$ k -grid for the supercell to be described later. To account for the correlation in Co(II) d -states, a static on-site U is used in the GGA+ U formalism[45]. Total energies are calculated self-consistently till the energy difference between successive steps was better than 10^{-5} eV. All results are sufficiently converged for this choice of basic computational parameters.

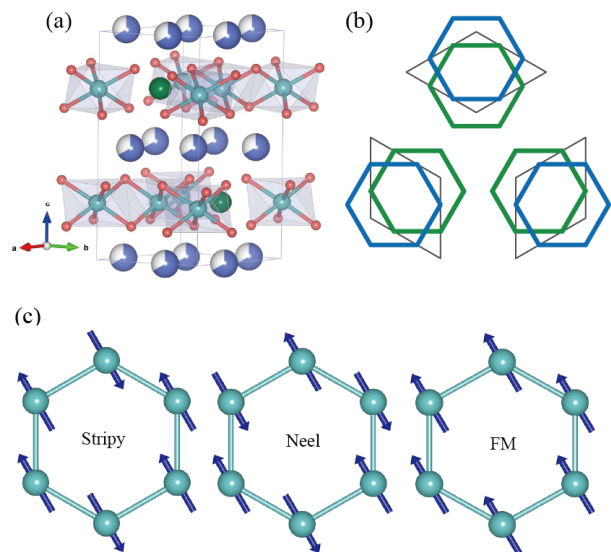


FIG. 1. Crystal and magnetic structures of $\text{Na}_2\text{Co}_2\text{TeO}_6$. (a) Crystal structure. Cyan, red and green balls represent Co, O and Te, respectively. (b) Top view of the lowest-energy Na network in two layers of $\text{Na}_2\text{Co}_2\text{TeO}_6$ unit cell obtained in our Cluster expansion model, in accordance with an average 2/3 occupancy of the Na sites. (c) Possible magnetic structures in a single-layer honeycomb lattice of Co atoms, showing the stripy, Néel and ferromagnetic configurations.

As shown in Fig. 1(a), in the experimental crystal structure of $\text{Na}_2\text{Co}_2\text{TeO}_6$ [12, 14, 15, 38–40] Co(II) ions are caged in edge-sharing oxygen octahedra, forming a honeycomb lattice with a Te ion sitting in the center of each hexagon. These 2-dimensional Co-O-Te sheets are joined by hexagonal close-packed Na monolayers to form a 3-dimensional array, with hexagonal lattice in the space group $P6_322$. It was found that the intercalated Na layers has a 2/3 overall occupancy, though the six-fold symmetry remains intact. Not only this presents a challenge to DFT calculations, the charge pattern of

the partially occupied Na layers can also influence the spin states and interactions which is the central topic of present study. Therefore, we begin by sorting out this issue before performing further analysis of the electronic and spin structures.

The total energy of $\text{Na}_2\text{Co}_2\text{TeO}_6$ with 2/3 Na occupancy is expressed as a cluster expansion up to the 4th order, as

$$E(\mathcal{C}) = E_0 + \sum_{\alpha} g_{\alpha} V_{\alpha} \varphi_{\alpha}, \quad (1)$$

where a configuration \mathcal{C} refers to particular occupation of the lattice conforming to 2/3 occupancy of a Na monolayer, V_{α} are the effective cluster interactions associated with the symmetry inequivalent cluster α with multiplicity g_{α} , and φ_{α} are the cluster correlations calculated as symmetrized averages of the products of all lattice sites (1, 2, 3 and 4 for one, two, three and four-point clusters) over the number of unit cells needed to form the cluster α in configuration $\{\mathcal{C}\}$. Cluster spaces with up to four-point clusters (quadruplets) comprised of 132 distinct clusters are considered. Further improvement on the model is not seen upon inclusion of higher order clusters.

The effective cluster interactions V_{α} are obtained using least absolute shrinkage and selection operator. [46] The total energies of $2 \times 2 \times 1$ supercell obtained from *ab initio* calculations are used to train and cross-validate the model in Eq.(1). The model is subsequently employed

in Monte Carlo simulations in the canonical ensemble to obtain the lowest energy configuration with Na vacancies. The Monte Carlo annealing processes start from a sufficiently high temperature of 1000 K, to avoid trapping into local minima. With lowering of temperature, we obtain the ground state at 300 K in each case which remain so with further lowering of temperature close to zero. Hence we set the lower temperature at 300 K in our Monte Carlo simulations. Typically, a system is annealed in $2^6 - 2^8$ steps, depending on system size, to avoid mode collapsing.

The Na monolayer with $n \times n$ supercells ($n = 4, 10, 14$) and random starting vacancy configurations conforming to 2/3 occupancy invariably converge to a honeycomb lattice, when annealed from over 1000 K steadily down to 300 K. The energy evolution for different supercells in the simulated annealing processes is shown in Fig. 2(a), which all evidently converge to the same ground state. The evolution of coordination numbers of Na for a 10×10 supercell during a typical annealing is shown in Fig. 2(b). The population of triply coordinated Na-sites increases gradually as the annealing proceeds, while the population of atoms with other coordination numbers diminish. The resultant structure at 300 K only has triply coordinated sites, corresponding to a honeycomb lattice. These results point to the honeycomb net as a most probable ground state monolayer configuration. However, when we stack two of such these honeycomb lattices together in a given experimental unit cell, where the original hexagonal close-packed sheets adopt a *ABAB* type periodic stacking, it is seen the unit cell cannot have 3-fold rotational symmetry. As shown in Fig. 1(b), the three replica of such bilayer stacking with a unit cell interrelated by C_3 rotations are shown. Clearly, these replica do not coincide with each other, demonstrating the lack of 3-fold symmetry in this ordered Na vacancy configuration.

We thus come to the following interpretation of the computed Na vacancy configuration, in order to reconcile with the experimentally established crystal structure with an apparent 3-fold symmetry. Within each layer, the Na vacancies are arranged to produce an ordered honeycomb lattice, and the layer stacking is disordered owing to weak interlayer interactions to produce an overall 3-fold symmetry in elastic scattering experiments. For example, for an in-plane reciprocal lattice vector $\mathbf{g} \cdot \mathbf{c} = 0$, the structure factor of the Na sublattice is

$$S(\mathbf{g}) = n \overline{\exp(-i\mathbf{g} \cdot \mathbf{d})},$$

where n is the atom number density, \mathbf{d} is the location of sodium in a 2-dimensional honeycomb sheet within a unit cell, and the overbar means averaging over all layers. Clearly, given the presumed stacking disorder, the three configurations in Fig. 1(b) contribute equally to the average and $S(\mathbf{g})$ shall have 3-fold symmetry.

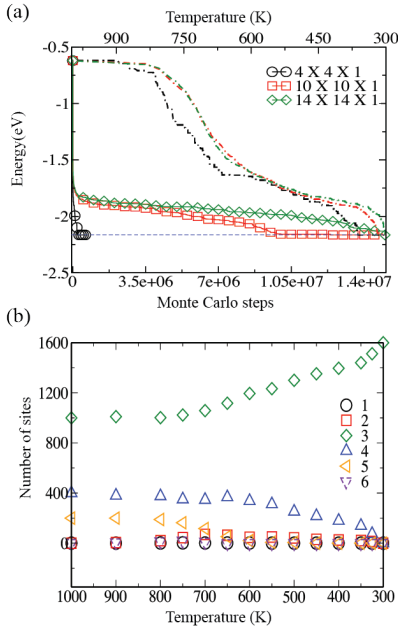


FIG. 2. (a) Variation in energy per atom with temperature (top three dashed lines) and with Monte Carlo steps (lower three solid lines) obtained in annealing process for various supercells. Horizontal dashed line represents the ground state energy. (b) Change in coordination of Na-sites with temperature for $10 \times 10 \times 1$ supercell.

B. Electronic structure

Therefore, we shall adopt one of the three equivalent Na configurations in Fig. 1(b) in the *ab initio* calculations. Note, however, that the 3-fold symmetry will be imposed on the TB Hamiltonian based on which magnetic interactions are extracted, to be discussed later. With this choice of vacancy configuration along with the experimentally observed zigzag magnetic ground state, a full structural optimization relaxing both ion positions and lattice parameters using $U = 3$ eV lead to lattice parameters within 1.4% of the experimental values. We hence use the experimental crystal structure in all subsequent *ab initio* band structure calculations.

Once the SOI is included self-consistently in our calculations in the structure described above, the experimentally proposed zigzag antiferromagnetic ground state can be reproduced. The total energy for various magnetic configuration is listed in Table I and shown in Fig. 1(c) (For zig-zag configuration, see Fig. 4(b)). The spin magnetic moments of Co atoms in the ground state were found to be $2.69 \mu_B$, comparable with the experimentally observed value of $2.77 \mu_B$ and a little smaller than what is expected for an effective 3/2-spin system.

Mag. config.	Spin-direction		
	010	001	100
Zig-zag	0.0	0.226	0.231
Stripy	0.338	1.688	0.116
Neel	0.724	0.737	0.758
FM	0.252	0.073	0.086

TABLE I. Energies of various magnetic configurations (in eV) relative to the zigzag antiferromagnetic configuration.

In order to extract the magnetic interactions, we now construct a TB Hamiltonian describing the low-energy states of both the materials, using the maximally localized Wannier function [47]. The mapping was done considering a basis formed by all the five d orbitals on Co atoms. The Brillouin zone of $\text{Na}_2\text{Co}_2\text{TeO}_6$ is shown in Fig. 3(a). The *ab initio* band structure for the non-magnetic phase shown in Fig. 3(b) in a calculation involving SOC shows that the low-energy excitation involves both the e_g and t_{2g} states. Thus the Wannier functions involve the full set of d orbitals on Co. Using the basis $\psi_{i\sigma}^\dagger = [d_{z^2}^\dagger, d_{xz}^\dagger, d_{yz}^\dagger, d_{x^2-y^2}^\dagger, d_{xy}^\dagger]_{i\sigma}$ for site i and spin σ , the TB Hamiltonian then reads

$$H_0 = H_{\text{cf}} + H_{\text{hop}} + H_{\text{soc}} \\ = \sum_{i,\sigma} \psi_{i\sigma}^\dagger \Delta_i \psi_{i\sigma} + \sum_{i \neq j, \sigma} \psi_{i\sigma}^\dagger T_{ij} \psi_{j\sigma} + \sum_i \lambda \mathbf{L}_i \cdot \mathbf{s}_i \quad (2)$$

in which the CF (Δ_i) and the hopping amplitudes (T_{ij}) are obtained from Wannier interpolation [47] of the *ab initio* spectrum without SOI. The so-determined spin-

independent CF matrix is

$$\Delta_i = \begin{bmatrix} 1.377 & 0.045 & 0.045 & 0.000 & 0.089 \\ 0.045 & 0.015 & 0.006 & 0.078 & -0.006 \\ 0.045 & 0.006 & 0.051 & -0.077 & -0.006 \\ 0.000 & 0.078 & -0.078 & 1.377 & 0.000 \\ 0.089 & -0.006 & -0.006 & 0.000 & 0.015 \end{bmatrix} \quad (3)$$

The spin-independent hopping amplitudes are listed in Appendix A.

The last term in Eq. (2) is the atomic SOI, and its strength $\lambda = 65$ meV is determined by fitting the SOC included *ab initio* band structure with a TB model after explicitly introducing the intratomic SOC term in the model. The band structure fit is shown in Fig. 3(b). It is observed that the SOI in $\text{Na}_2\text{Co}_2\text{TeO}_6$, λ is considerably smaller than that in Ir- and Ru-based materials, for which $\lambda \approx 400$ meV [48] and 150 meV [18], respectively.

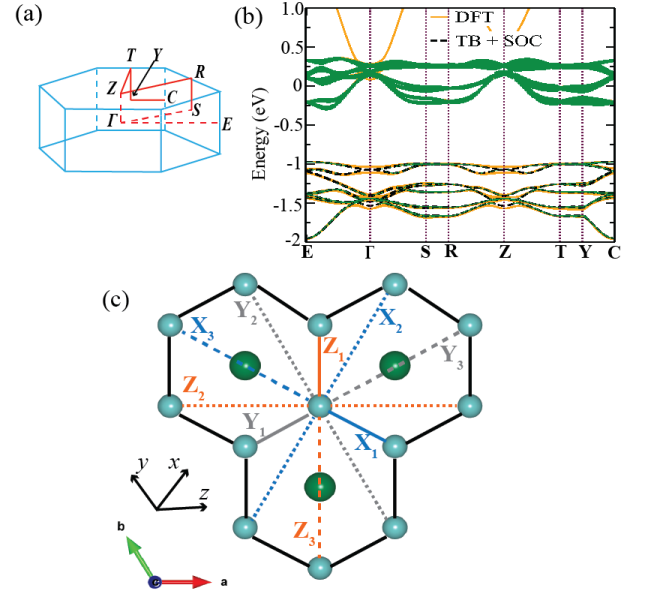


FIG. 3. (a) Brillouin zone of $\text{Na}_2\text{Co}_2\text{TeO}_6$. (b) *Ab initio* band structure with SOC fitted with TB Hamiltonian with SOI. The fat band representation depicts e_g components. The Fermi energy is set to zero. (c) A single-layer Co^{+2} lattice in $\text{Na}_2\text{Co}_2\text{TeO}_6$. 1NN, 2NN and 3NN bonds are indicated by solid, dotted and dashed lines, respectively. Orange, dark gray and skyblue color represent the Z, Y and X bonds, respectively. a , b and c are the crystallographic axes and cubic axes of Co-O octahedra are denoted by x , y and z .

C. Magnetic interaction and magnetism

Before investigating in detail the magnetic properties of $\text{Na}_2\text{Co}_2\text{TeO}_6$, it is important to discuss its structural and electronic features. A comparison between $\text{Na}_2\text{Co}_2\text{TeO}_6$ and previously studied 4/5d materials with pseudospin-1/2 ground state highlights following crucial differences between these materials. Additional presence

of e_g orbitals for $\text{Co}^{+2}-d^7$ with active spin only degree of freedom put this material in a different class when compared to the materials with d^5 configuration. Also, magnitude of trigonal CF in $\text{Na}_2\text{Co}_2\text{TeO}_6$ (~ 27 meV, see the matrix in Eq. [3]) is expected to be of the same order as that of the SOC strength (λ) which further distinguishes this material from those of $4d/5d$ based compounds where λ is an order of magnitude larger than the trigonal CF. As λ is responsible for energy separation between $J_{\text{eff}}=1/2$ and $J_{\text{eff}}=3/2$ states while trigonal CF mixes these states, this separation is expected to be smaller in $\text{Na}_2\text{Co}_2\text{TeO}_6$.

From a structural perspective, Co-O-Co angles across a pair of edge-sharing octahedra are $\sim 92^\circ$ which is close to the ideal case of 90° . In contrast, the same metal-ligand-metal bond angles in Na_2IrO_3 and RuCl_3 are significantly larger: 100° for the former and 94° for the latter [17, 22]. This difference manifests itself in terms of enhanced direct (σ -type) hopping amplitudes between d orbitals of Co atoms [49]. For example, in Appendix A, $d_{yz} - d_{yz}$ hopping on a X bond is larger when compared to other hopping interactions. The same is true for $d_{zx} - d_{zx}$ and $d_{xy} - d_{xy}$ hopping on Y and Z bonds. Opposite has been observed in case of Na_2IrO_3 [49].

To be concrete, let's consider the interaction Hamilto-

nian

$$H_{\text{int}} = \frac{U}{2} \sum_{i,\alpha} n_{i\alpha\sigma} n_{i\alpha\sigma'} + \frac{U'}{2} \sum_{i,\alpha \neq \beta} n_{i\alpha} n_{i\beta} - \frac{J_{\text{H}}}{2} \sum_{i,\sigma,\sigma',\alpha \neq \beta} \psi_{i\alpha\sigma}^\dagger \psi_{i\alpha\sigma'} \psi_{i\beta\sigma'}^\dagger \psi_{i\beta\sigma} - \frac{J'}{2} \sum_{i,\sigma \neq \sigma',\alpha \neq \beta} \psi_{i\alpha\sigma}^\dagger \psi_{i\beta\sigma'} \psi_{i\alpha\sigma'}^\dagger \psi_{i\beta\sigma} \quad (4)$$

Here, U/U' are intraorbital/interorbital Hartree energies; and J_{H} and J' are Hund's coupling and pair hopping interaction, respectively. Rotational invariance in the single atom limit dictates the relationships: $U' = U - 2J_{\text{H}}$ and $J_{\text{H}} = J'$.

The key here is the d^7 manifold has a two-fold degenerate ground state, which form a Kramers doublet and can be treated as a pseudospin-1/2. In order to extract the magnetic interactions of these pseudospin states, we first project the full TB Hamiltonian onto the pseudospin $J_{1/2}$ space $\{\phi_{i\alpha}\}$, $\alpha = \uparrow, \downarrow$, where \uparrow, \downarrow refer to the SOC pseudospin-1/2 states. We start in the isolated atom limit, where $H_{\text{atom}} = H_{\text{cf}} + H_{\text{soc}} + H_{\text{int}}$, and introduce the hopping contribution H_{hop} as a perturbation. In the second-order perturbation theory, the Hamiltonian is written as,

$$H^{(2)} = \sum_{ij} \sum_{\alpha\beta\alpha'\beta'} \mathcal{H}(i,j)_{\alpha\beta\alpha'\beta'} |i\alpha, j\beta\rangle \langle i\alpha', j\beta'|, \quad (5)$$

$$\mathcal{H}(i,j)_{\alpha\beta\alpha'\beta'} = \sum_{kl} \sum_{\gamma\lambda} \frac{1}{\Delta E} \langle i\alpha, j\beta | H_{\text{hop}} | k\gamma, l\lambda \rangle \langle k\gamma, l\lambda | H_{\text{hop}} | i\alpha', j\beta' \rangle, \quad (6)$$

where $1/\Delta E = \frac{1}{2}[1/(E_{i\alpha} + E_{j\beta} - E_{k\lambda} - E_{l\gamma}) + 1/(E_{i\alpha'} + E_{j\beta'} - E_{k\lambda} - E_{l\gamma})]$. Here, $|i\alpha, j\beta\rangle$ and $|i\alpha', j\beta'\rangle$ are two-site states in the $J_{1/2}$ ground states, and $|k\lambda, l\gamma\rangle$ are two-site excited states, both in the isolated atom limit. H_{hop} connects a two-site ground state to an excited state with (d^6, d^8) configuration, the dimensions of whose Hilbert spaces are 210 and 45, respectively. The eigenstates of isolated Co with 6, 7 and 8 d electrons are obtained by exact diagonalization.

Considering the scenario when magnitude of Hubbard U and CF splitting are much larger than the hopping amplitudes and also when the SOC strength is much larger than t^2/U , the low energy space is formed by the lowest two degenerate many body states of the "onsite" Hamiltonian (H_{atom}). These states behaves exactly as pseudospin-1/2 Kramers doublet in the limit of an infinite CF and in the absence of any lattice distortions which can further split the t_{2g} orbitals such as trigonal

distortions. Writing the pseudospin $J_{1/2}$ as $S^\mu = \frac{1}{2}\sigma^\mu$, Eq. (6) can be mapped to a spin Hamiltonian of the form

$$H_{\text{spin}} = S_i^\mu \Gamma(i,j)^{\mu\nu} S_j^\nu = \frac{1}{4} \Gamma(i,j)^{\mu\nu} \phi_{i\alpha}^\dagger \sigma_{\alpha\alpha'}^\mu \phi_{i\alpha'} \phi_{j\beta} \sigma_{\beta\beta'}^\nu \phi_{j\beta}^\dagger, \quad (7)$$

where $\mu, \nu = 0, x, y, z$, σ^μ are Pauli matrices, and summation over all repeated indexes is implied. The map can be achieved by solving the linear equations

$$-\frac{1}{4} \sigma_{\alpha\alpha'}^\mu \sigma_{\beta\beta'}^\nu \Gamma(ij)^{\mu\nu} = \mathcal{H}(i,j)_{\alpha\beta\alpha'\beta'} \quad (8)$$

The spin Hamiltonian thus can be rewritten as,

$$\begin{aligned}
H_{\text{spin}} = & \sum_{\langle i,j \rangle \in l(mn)} [J_1^l \boldsymbol{\sigma}_i \cdot \boldsymbol{\sigma}_j + K_1^l \sigma_i^l \sigma_j^l] \\
& + \eta_1^l (\sigma_i^m \sigma_j^n + \sigma_i^n \sigma_j^m) \\
& + \eta_1^l (\sigma_i^m \sigma_j^l + \sigma_i^n \sigma_j^l + \sigma_i^l \sigma_j^m + \sigma_i^l \sigma_j^n) \\
& + \sum_{\langle\langle i,j \rangle\rangle \in l(mn)} [J_3^l \boldsymbol{\sigma}_i \cdot \boldsymbol{\sigma}_j + K_3^l \sigma_i^l \sigma_j^l] \\
& + \eta_3^l (\sigma_i^m \sigma_j^n + \sigma_i^n \sigma_j^m) \\
& + \eta_3^l (\sigma_i^m \sigma_j^l + \sigma_i^n \sigma_j^l + \sigma_i^l \sigma_j^m + \sigma_i^l \sigma_j^n)
\end{aligned} \quad (9)$$

Above $\langle i,j \rangle / \langle\langle i,j \rangle\rangle$ represent 1NN/3NN pairs. The 2NN interaction is omitted as they are negligibly small. J , K and η are, respectively, the Heisenberg, Kitaev and off-diagonal interactions on any $l \in \text{Z/X/Y}$ bond. E.g., for Z-type bond, (mn) is (xy) and so on.

We now comment briefly on the results obtained from diagonalization of the “onsite” Hamiltonian, $H_{\text{atom}} = H_{\text{cf}} + H_{\text{soc}} + H_U$, before going into a detailed discussion of the magnetic interactions in $\text{Na}_2\text{Co}_2\text{TeO}_6$.

1. Onsite Hamiltonian: H_{atom}

There are four parameters in H_{atom} viz, U , J_{H} , λ and Δ . From the optical spectra on CoO [50], estimated value of Hund’s splitting (J_{H}) is ~ 0.8 eV. J_{H}/U ratio in cobaltates is believed to be < 0.2 [10], hence $U = 5$ eV was initially fixed in our calculation of magnetic interactions. $\lambda = 65$ meV obtained from band structure fitting is slightly larger than an estimated value of ~ 0.015 eV (corresponding to $J_{\text{eff}}=1/2$ to $J_{\text{eff}}=3/2$ transition) from inelastic neutron scattering experiment [12]. Later, we will vary both U and λ to examine their effect on the magnetic interactions. Δ obtained from the atomic Hamiltonian of the TB model is consistent with what is expected for such materials [10, 13].

The energy separation between $J_{\text{eff}}=1/2$ and $J_{\text{eff}}=3/2$ states, obtained after diagonalizing H_{atom} with above mentioned parameter values, is ~ 24 meV which is in close agreement with the experimentally observed value of ~ 21 meV in $\text{Na}_2\text{Co}_2\text{TeO}_6$ [12], and is much smaller than the expected value of ~ 100 meV corresponding to $\frac{3}{2}\lambda$ (for $\lambda=0.065$ eV). We attribute this difference to be arising from large mixing between $t_{2g}-e_g$ orbitals through the trigonal distortions present in $\text{Na}_2\text{Co}_2\text{TeO}_6$. Compression of Co-O octahedra along c -axis causes large deviation of O-Co-O angles from the ideal 90° with the smallest and largest angles being $\sim 78^\circ$ and 97° , respectively. This non-orthogonal local environment causes mixing between different d orbitals. It is worth mentioning here that estimate of λ from experiments would yield a value of 15 meV and yet we obtained $J_{\text{eff}}=1/2 - 3/2$ separation consistent with experimentally observed value using $\lambda=65$ meV. This calls for scrupulous attention while estimating λ in the systems with active

e_g orbitals and large trigonal distortions. The $J_{\text{eff}}=3/2$ states were found to split into two doublets with an energy separation of ~ 7 meV. To examine the effect of “imperfect” CF due to additional trigonal distortions, we compare the result to a perfect octahedral geometry with $\Delta = 1.36$ eV. In this case, $J_{\text{eff}}=1/2$ and $J_{\text{eff}}=3/2$ separation increased to 34 meV while the $J_{\text{eff}}=3/2$ states regained their four fold degeneracy. Although the CF heavily mixes $J_{\text{eff}}=1/2-3/2$ states, pseudospin-1/2 picture is still relevant in $\text{Na}_2\text{Co}_2\text{TeO}_6$ as both, the U and CF splitting $\Delta_{t_{2g}-e_g}$ are much larger than the hopping amplitudes (t) and $\lambda \gg t^2/U$ still holds in our case.

2. Magnetic interactions

The magnetic interaction on X/Y/Z bonds (see Fig. 3(c)), estimated from the process described above, are tabulated in Table II. Owing to the local site symmetry C_3 , we have identical magnetic interactions on all the three bonds. Indeed, the 1NN Heisenberg term is highly suppressed and antiferromagnetic as was expected in this case due to opposite sign of e_g-e_g and $t_{2g}-e_g$ exchange process [10, 13]. However, contrary to the previous speculations, the ferromagnetic Kitaev term is also small and found to be an order of magnitude smaller when compared with recent experimental estimation from the fitting of spin-wave dispersion data [12]. The same is true for a comparison with Ru [36] and Ir [35] based compounds. There can be mainly two reasons behind such a reduction. First, smaller hopping amplitudes and large U in our case when compared to $4d/5d$ materials can contribute to this huge reduction. The effect of the latter is verified by reducing U to 2.5 eV while keeping the J_{H}/U ratio fix at 0.16, in which case the magnitude of both J_1 and K_1 are substantially enhanced, to 1.93 and -1.616 meV, respectively. The other factor contributing to the reduction is the weaker SOI in $\text{Na}_2\text{Co}_2\text{TeO}_6$. We will examine the effect of varying λ in a later section to understand how it affects the magnetic interactions.

Bond type	First NN			Third NN		
	J	K	η/η'	J	K	η/η'
X/Y/Z	0.261	-0.678	0.0	3.153	-0.04	0.76

TABLE II. Estimated 1NN and 3NN Heisenberg J , Kitaev K and off-diagonal η , η' terms in $\text{Na}_2\text{Co}_2\text{TeO}_6$ given in meV. The 2NN interactions as well as terms other than J and K for 1NN were found to be negligibly small. Parameters used are $U = 5$ eV, $J_{\text{H}} = 0.8$ eV and $\lambda = 65$ meV.

Interestingly, all other first-neighbour off-diagonal spin interactions η_1 and η'_1 are found to be negligibly small for this particular set of parameters, in contrast to what was obtained for Ir- [35] and Ru- based [36] compounds. Previous arguments for the suppression of the Heisenberg interaction in this material also apply to these off-diagonal interactions. We find the second-neighbour as well as inter-layer coupling to be negligibly small, ruling

out the possibility of any inter-layer interactions and effect of Na-vacancies which separates these Co-hexagons in c -direction. This again is in complete agreement with the recent experimental observation of negligible inter-layer spin interactions [15]. Not to a complete surprise, the 3NN in $\text{Na}_2\text{Co}_2\text{TeO}_6$ are also non-zero, similar to the cases of iridates and RuCl_3 [35, 36].

Surprisingly, however, antiferromagnetic J_3 is larger in magnitude than K_1 , hence being the dominant interaction in $\text{Na}_2\text{Co}_2\text{TeO}_6$. At first glance, it seems unusual given that $3d$ orbitals are more compact compared to their $4d/5d$ counterparts. In $\text{Na}_2\text{Co}_2\text{TeO}_6$, the 3NN hopping can be mediated via Te ions sitting at the center of a Co-hexagon. Orbital projected density of states for Te- s/p orbitals (not shown) precludes any significant contribution near the Fermi-level where Co- d and O- p have their main contributions. This rules out any direct interaction between Co- d and Te- s/p orbitals. A second possibility for the 3NN interaction is through shared O- p orbitals between these ions, which is favored by the highly suppressed 3NN Kitaev interaction due to a cancellation of anisotropic interactions from multiple long-distance pathways. This then allows J_3 to become the largest magnetic interaction in this compound. Off-diagonal couplings of a smaller magnitude appears on these bonds. On a Z-bond, η_3 is found to be antiferromagnetic, while η'_3 ferromagnetic. However, on X or Y bond, signs of these couplings do not follow a specific pattern. On these two bonds, η'_3 never becomes ferromagnetic while η_3 can be either ferro- or antiferro-magnetic.

In order to examine whether the obtained parameters can reproduce the magnetic ground state of $\text{Na}_2\text{Co}_2\text{TeO}_6$, we optimize the magnetic structure using Hamiltonian of Eq. (9) with spins allowed to rotate in the a - b plane. We find that the classical ground state was zigzag-type with the ferromagnetic chains running along a -direction coupled antiferromagnetically in direction perpendicular to a (see Fig. 4(c)) with propagation vector $\sim (0.0, 0.5, 0.0)$. We call it Z2 structure. This structure is different than the experimentally proposed magnetic structure with propagation vector $(0.5, 0.0, 0.0)$ which we call Z1. However, in the next section we show that one can also obtain Z1 as the classical ground by tuning the parameters of perturbation theory.

3. Phase diagram

We varied U and SOC strength (λ) to study their effect on magnetic interactions and on the ground state. A phase diagram, obtained from optimization of classical ground with magnetic interactions obtained at different U - λ values, is shown in Fig. 4(a). J_H/U ratio has been kept fixed at 0.16 in all these calculations. We obtain four distinct phase viz, Neel and three types of zigzag magnetic order (Fig. 4(b)/(c)/(d)) differentiated by direction of antiferromagnetic coupling between the ferromagnetic chains. Phase diagram can be read in the following man-

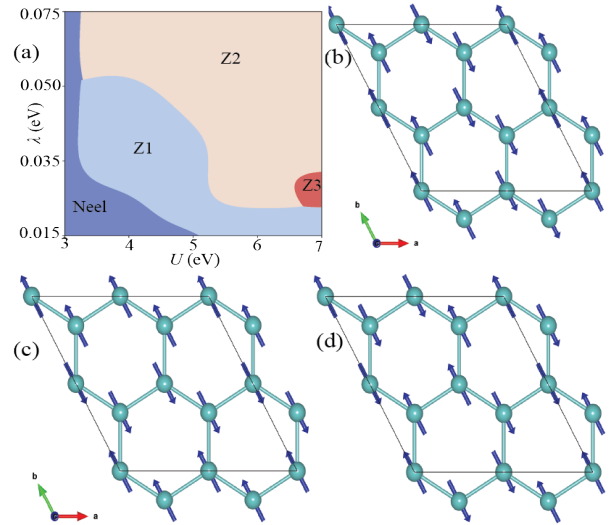


FIG. 4. (a) The U - λ phase diagram for $\text{Na}_2\text{Co}_2\text{TeO}_6$ at $J_H/U = 0.16$. Four distinct phases, Neel, (b) experimentally proposed magnetic state zigzag 1 (Z1), (c) zigzag 2 (Z2) and (d) zigzag 3 (Z3), can be obtained after optimization of classical ground state.

ner.

In a smaller U range (close to 3 eV), classical magnetic ground state is Neel-type and independent of λ . In this region, antiferromagnetic J_1 is dominant over other types of first neighbour interactions. All these interactions increase with increase in λ with K_1 more rapidly than J_1 . At a particular λ , with the increase in U , we find decreasing J_1 and K_1 with J_1 decreasing more rapidly than K_1 . After critical values of U and λ , situated on the phase boundary of Neel-Z1/Z2 phase, K_1 term starts to compete with J_1 . Only when $K_1 \geq J_1$, the magnetic ground state changes from Neel to one of the zigzag types. Z1 configuration (Fig. 4(b)) with propagation vector $\sim (0.5, 0.0, 0.0)$ is the experimentally observed magnetic state of $\text{Na}_2\text{Co}_2\text{TeO}_6$. In Z3 configuration (Fig. 4(d)) with propagation vector $\sim (0.5, 0.5, 0.0)$, antiferromagnetic coupling between ferromagnetic zigzag layers is along $(1\ 1\ 0)$ direction. At some of the phase points, spin moments of our classical ground state was found to slightly deviate from b -direction owing to small η/η' terms.

Here, a couple of remarks are in order. First, neither J_1 , K_1 terms nor J_3 , η_3/η'_3 terms alone can produce the zigzag ground state of $\text{Na}_2\text{Co}_2\text{TeO}_6$ which is a collective efforts of all these terms. Second, these three zigzag spin configurations are distinct and hence break the three fold rotational symmetry. To verify this point we compared the energies of these three configurations at same phase point, $U = 4$ eV and $\lambda = 0.60$ eV, the phase boundary point between Z1 and Z2 configurations. At this point, the obtained magnetic ground state was Z1 type and energies of Z2 and Z3 configurations were higher in energy by 0.010 meV and 0.015 meV per spin. These differences, when compared with the scale of magnetic

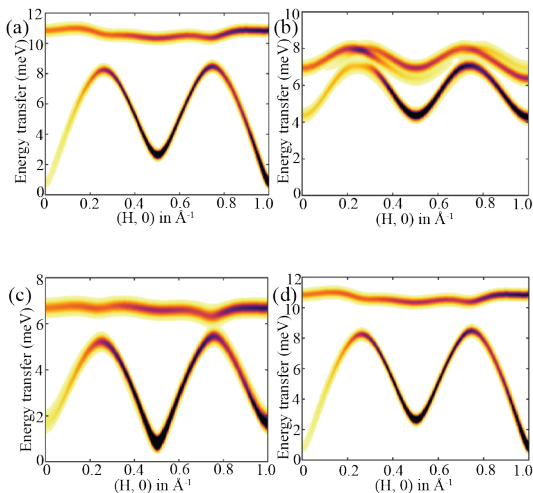


FIG. 5. Spin wave spectra obtained from linear spin wave theory for (a) Neel ($U = 3.25$ eV, $\lambda = 0.065$ eV), (b) Z1 ($U = 4$ eV, $\lambda = 0.06$ eV), (c) Z2 ($U = 5$ eV, $\lambda = 0.065$ eV) and (d) Z3 ($U = 7$ eV, $\lambda = 0.025$ eV).

coupling strengths, are significant and hence establish the fact of these three zigzag magnetic configurations being distinct. Our three zigzag configurations differ from those proposed in Chen *et.al.* [38] as in the latter, the three domains of zigzag configurations are related by three fold rotational symmetry. For further validation of our obtained magnetic interactions, spin-wave spectra are computed and analyzed next.

D. Spin wave spectra

Recently, several inelastic neutron scattering experiments on $\text{Na}_2\text{Co}_2\text{TeO}_6$ have reported spin wave spectra of this material [12, 15]. The main feature of these reported spectra is gapped dispersive modes with lowest dispersive branch of width around 3 meV and some flat modes around 4.5 meV and 7 meV. A natural question about how well our estimated magnetic interactions can reproduce these experimental findings is inevitable. The spin Hamiltonian in Eq. (9) with estimated magnetic interactions is solved using the linear spin wave theory to obtain the spin wave spectra [51]. These calculations were performed for the four distinct magnetic phases in Fig. 4(a), and are shown in Fig. 5.

The spectra of Néel, Z1 and Z3 states were found to differ from the experimentally obtained ones. First, dispersion width of the lowest branch in the spectra of Néel and Z3 phases (Fig. 5(a) and (d)) is much larger (~ 8 meV) than the experimentally observed ~ 3 meV. Though this experimental feature of the spectra is captured in the case of Z1 phase (Fig. 5(b)), a gap of ~ 1 meV with next higher dispersive mode observed in the experiments is missing in this case. Also, this gap is much larger (more than 2 meV) in our calculated spectra for Neel and Z3

phases. Therefore, our calculated spin wave spectra for the Z2 phase shown in Fig. 5(c) closely resembles the experimental ones. Though, the band width of lowest branch is slightly higher (~ 5 meV) in our model, it reproduces the gap of ~ 1 meV with next higher branch, consistent with experimental findings [12].

III. $\text{Na}_3\text{Co}_2\text{SbO}_6$

As for $\text{Na}_3\text{Co}_2\text{SbO}_6$, Co-O-Sb environment is similar to that of Co-O-Te in $\text{Na}_2\text{Co}_2\text{TeO}_6$, with only difference of 2-dimensional sheets of Co-O-Sb are joined by a triangular lattice of Na atoms in formation of three-dimensional lattice along c direction with space group $C2/m$. It has also the zigzag type antiferromagnetic ground state described by propagation vector $(1/2, 1/2, 0)$ with the spins aligned along the crystallographic b axis. The Brillouin zone of $\text{Na}_3\text{Co}_2\text{SbO}_6$ is shown in Fig. 6(a). We extracted the CF matrix and hopping interactions for $\text{Na}_3\text{Co}_2\text{SbO}_6$ in similar fashion as we did in case of $\text{Na}_2\text{Co}_2\text{TeO}_6$ i.e. by fitting the *ab initio* band structure for $\text{Na}_3\text{Co}_2\text{SbO}_6$ i.e. by fitting the *ab initio* band structure to a Wannier TB model and fitting is shown in Fig. 6(b).

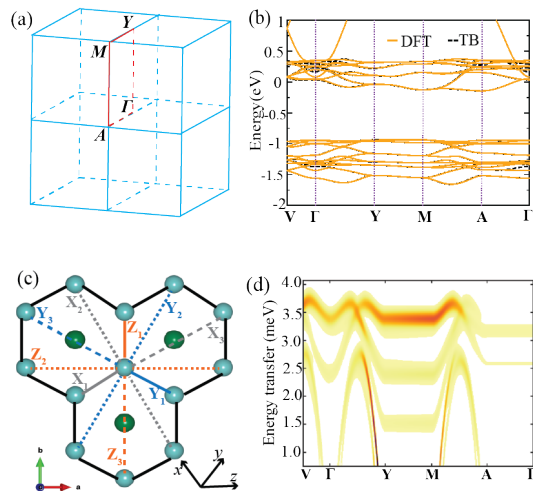


FIG. 6. (a) Brillouin zone of $\text{Na}_3\text{Co}_2\text{SbO}_6$. (b) TB fitting of *ab initio* band structure of $\text{Na}_3\text{Co}_2\text{SbO}_6$. (c) Lattice of Co^{+2} in $\text{Na}_3\text{Co}_2\text{SbO}_6$. 1NN, 2NN and 3NN are shown by solid, dotted and dashed lines. Orange, dark gray and skyblue color represent the Z, X and Y bonds respectively. a , b and c are the crystallographic axes and cubic axes of Co-O octahedra are denoted by x , y and z . (d) Spin wave spectra obtained from linear spin wave theory for optimized classical ground state of $\text{Na}_3\text{Co}_2\text{SbO}_6$ (at $U = 5.0$ eV, $\lambda = 0.065$ eV)

The obtained CF matrix and hopping amplitudes are given in Eq. 10 and Appendix B, respectively. Inspection of O-Co-O angles in an octahedra reveal a deviation from ideal case of 90° to the largest angle being $\sim 96^\circ$ and smallest one is $\sim 81^\circ$. Thus, the lower symmetry of $C2/m$ space group along with the trigonal CF causes the additional splitting of 15 meV within e_g orbitals and two types of splitting within 6 meV, 12 meV

splitting within the t_{2g} orbitals. This is consistent with the previous findings on Iridates [35] and RuCl_3 [36]. Co-O-Co angles across a pair of edge-sharing octahedra are $\sim 93.5^\circ$, again close to 90° but slightly larger than the case of $\text{Na}_2\text{Co}_2\text{TeO}_6$. In our “onsite” Hamiltonian for $\text{Na}_3\text{Co}_2\text{SbO}_6$, U and λ were kept the same to 5 eV and 65 meV as before. Similar to the case of $\text{Na}_2\text{Co}_2\text{TeO}_6$, in this case too, lowest six states are three Kramer’s doublet with energy separation of 28 and ~ 13 meV, between the lowest and the higher two doublets, respectively.

$$\Delta_i = \begin{bmatrix} 1.344 & 0.133 & -0.035 & 0.002 & -0.084 \\ 0.133 & 0.046 & 0.007 & -0.180 & 0.020 \\ -0.035 & 0.007 & 0.016 & -0.093 & 0.022 \\ 0.002 & -0.180 & -0.093 & 1.309 & -0.224 \\ -0.084 & 0.020 & 0.022 & -0.224 & 0.045 \end{bmatrix} \quad (10)$$

For the lower symmetry space group of $\text{Na}_3\text{Co}_2\text{SbO}_6$, symmetry inequivalent nearest neighbour bonds are of two types, *viz-a-viz*, Z_1 bonds \parallel to crystallographic b axis with C_{2h} point group symmetry and X_1/Y_1 bonds lying in the ab plane with lower C_i point group symmetry. This arrangement of bonds is shown in Fig. 6(c). In such a case, on these X/Y type bonds, in addition to J , K , Γ and Γ' , one needs additional parameters ζ and ξ as explained in Winter *et. al.* [35] to describe the magnetic interactions. Magnetic interactions estimated in this case using second order perturbation method is listed in Table III. By comparing with $\text{Na}_2\text{Co}_2\text{TeO}_6$, we find that the 1NN magnetic interactions are more or less similar in this case. However, a subtle difference can be found for the 3NN interactions as in $\text{Na}_3\text{Co}_2\text{SbO}_6$, the magnitudes are half of their values of $\text{Na}_2\text{Co}_2\text{TeO}_6$. One more difference between these two materials is that the Kitaev coupling on Z_3 bond, though again smaller, is found to be antiferromagnetic in this case. Additionally, the η_3/η'_3 terms are much smaller (almost half) in this case when compared to $\text{Na}_2\text{Co}_2\text{TeO}_6$. With these magnetic parameters, optimization of classical ground state using the Hamiltonian in Eq. 9 brings the same zigzag type magnetic ground which was obtained experimentally. However, we find a small deviation of spin from b direction along a -axis in our optimized structure in this case too. In terms of propagation vector, the optimized magnetic structure is described by $\sim (0.498, 0.492, 0)$. Using this optimized magnetic structure we calculated the spin wave spectra of $\text{Na}_3\text{Co}_2\text{SbO}_6$ shown in Fig. 6(d). Most of the intensity of this spectra is found in 3-4 meV energy range which is in reasonably good agreement with the recent experiment [12].

We now will briefly compare the properties of these two materials. Structurally, the crucial difference is the stacking of the Co honeycomb layers. For $\text{Na}_2\text{Co}_2\text{TeO}_6$, the layers are staggered while for $\text{Na}_3\text{Co}_2\text{SbO}_6$, these layers are exactly on the top of each other. However, the estimated interlayer magnetic interactions in our calculations are found to be negligibly small ruling out any possibility of coupling between the honeycomb layers of

Bond type	J	K	η	η'	ξ	ζ
Z_1	0.3	-0.757	0.0	0.0	0.0	0.0
X_1/Y_1	0.186	-0.211	0.0	-0.15	-0.421	0.0
Z_3	1.7	0.4	0.34	-0.31	0.0	0.0
X_3/Y_3	1.823	-0.189	0.31	0.0	-0.211	0.302

TABLE III. Estimated first and third NN Heisenberg J , Kitaev K and off-diagonal η, η' terms with additional parameters ξ and ζ in $\text{Na}_3\text{Co}_2\text{SbO}_6$ given in meV. The 2NN interactions were found to be negligibly small. Parameters used are $U = 5$ eV, $J_H = 0.8$ eV and $\lambda = 65$ meV.

Co in both these materials. Co-Co distance in these two materials is very similar and comparatively larger deviation of Co-O-O angle from 90° between edge shared octahedra is found in $\text{Na}_3\text{Co}_2\text{SbO}_6$ ($\sim 93.5^\circ$) when compared to the $\text{Na}_2\text{Co}_2\text{TeO}_6$ (92°) [14] as discussed earlier. This small difference does not seem to substantially affect the nearest neighbour magnetic interactions. So, while 1NN interactions have similar strengths in both the materials (after averaging of two type of bonds in $\text{Na}_3\text{Co}_2\text{SbO}_6$), smaller 3NN magnetic interactions in $\text{Na}_3\text{Co}_2\text{SbO}_6$ can be the reason behind its lower T_N (~ 7 K) than $\text{Na}_2\text{Co}_2\text{TeO}_6$ ($T_N \sim 18$ K). Also, the smaller off-diagonal η_3/η'_3 in $\text{Na}_3\text{Co}_2\text{SbO}_6$ can be seen as a manifestation of the lower trigonal CF in $\text{Na}_3\text{Co}_2\text{SbO}_6$ as been explained in Liu *et. al.* [13]. Thus, smaller “undesirable” off-diagonal and 3NN terms makes $\text{Na}_3\text{Co}_2\text{SbO}_6$ a more suitable candidate than $\text{Na}_2\text{Co}_2\text{TeO}_6$ in the quest of spin-liquid behaviour.

In a recent study by Das *et. al.* [52] on cobalt-based Kitaev materials, the authors commented, en passant, on the magnetic interactions in $\text{Na}_3\text{Co}_2\text{SbO}_6$. They found 1NN ferromagnetic Heisenberg and off-diagonal, antiferromagnetic 1NN Kitaev and 3NN Heisenberg couplings, all are of equal strength for this compound, differing from our results. It is important to verify that the combination of their magnetic interactions stabilizes the zigzag ground state, from following two considerations. First, the consensus seems to be that the zigzag ground state in these materials is a result of a combination of ferromagnetic K_1 and antiferromagnetic J_1 and J_3 [10, 13]. Second, though with 1NN antiferro Kitaev coupling where the nature of Heisenberg term is of lesser consequence, one may also realize zigzag ground state. However, in this case role of longer-range Heisenberg interaction is to be clarified [10, 13].

IV. Summary and remarks

In this paper, we investigated the structural and magnetic properties of $\text{Na}_2\text{Co}_2\text{TeO}_6$ and $\text{Na}_3\text{Co}_2\text{SbO}_6$. Using a Cluster-expansion model, we find a particular pattern of hexagonal lattice formation by Na-vacancies in $\text{Na}_2\text{Co}_2\text{TeO}_6$. Using multiband Hubbard model and sec-

ond order perturbation theory, in the large U limit, we estimated the magnetic interactions in these material and show that a zigzag magnetic order can only be stabilized when Kitaev term is either comparable or larger than the first neighbour Heisenberg term. However, we find the third neighbour Heisenberg interaction to most dominant magnetic interactions in both these compounds. In addition, we also presented a phase diagram for $\text{Na}_2\text{Co}_2\text{TeO}_6$ by varying U and λ and find that a major portion of this phase diagram has different zigzag magnetic ground state. Based on the spin Hamiltonian, we calculated spin wave spectra and showed that our findings are in qualitative agreement with the recent neutron-scattering experiments. A comparison between these two

materials establish the fact that $\text{Na}_3\text{Co}_2\text{SbO}_6$ is might be a better candidate than $\text{Na}_2\text{Co}_2\text{TeO}_6$ in the quest for Kitaev materials due to smaller off-diagonal and 3NN magnetic interactions in the former.

Trigonal CF present in these materials is believed to be the main hurdle behind realization of a quantum spin liquid phase and has been recently suggested as an experimentally tuneable parameter [13]. Previously, this type of tuning has been achieved experimentally by means of strain in CoO [53] and would an interesting future direction of research at both theoretical and experimental fronts. Another interesting aspect from experimental perspective would be to investigate whether similar to $\alpha\text{-RuCl}_3$ [54], magnetic field can induce a quantum spin liquid phase in these cobalt-based compounds.

Appendix A. 1NN and 3NN hopping amplitudes in $\text{Na}_2\text{Co}_2\text{TeO}_6$

Hopping	1^{st} NN			3^{rd} NN		
	X	Y	Z	X	Y	Z
$d_{z2} \rightarrow d_{z2}$	-0.0307	-0.0307	-0.0709	0.0806	0.0806	-0.0335
$d_{zx} \rightarrow d_{zx}$	0.0364	-0.1699	0.0364	0.0047	-0.0327	0.0047
$d_{yz} \rightarrow d_{yz}$	-0.1699	0.0364	0.0364	-0.0327	0.0047	0.0047
$d_{x^2-y^2} \rightarrow d_{x^2-y^2}$	-0.0575	-0.0575	0.0046	0.0046	0.0046	0.1187
$d_{xy} \rightarrow d_{xy}$	0.0364	0.0364	-0.1699	0.0047	0.0047	-0.0327
$d_{z2} \leftrightarrow d_{zx}$	-0.0184	0.0638	0.0071	0.0082	0.0080	-0.0010
$d_{z2} \leftrightarrow d_{yz}$	0.0638	-0.0184	0.0071	0.0085	0.0073	-0.0010
$d_{z2} \leftrightarrow d_{x^2-y^2}$	0.0232	-0.0232	0.0000	0.0659	-0.0659	0.0000
$d_{z2} \leftrightarrow d_{xy}$	-0.0114	-0.0114	0.1275	0.0072	0.0063	0.0161
$d_{zx} \leftrightarrow d_{yz}$	0.0467	0.0467	-0.0457	-0.0007	-0.0007	-0.0077
$d_{zx} \leftrightarrow d_{x^2-y^2}$	-0.0030	0.1104	-0.0176	0.0030	0.0146	0.0089
$d_{zx} \leftrightarrow d_{xy}$	0.0457	-0.0467	-0.0467	0.0077	0.0007	0.0006
$d_{yz} \leftrightarrow d_{x^2-y^2}$	-0.1098	0.0030	0.0176	-0.0139	-0.0036	-0.0089
$d_{yz} \leftrightarrow d_{xy}$	-0.0479	0.0457	-0.0467	0.0006	0.0077	0.0006
$d_{x^2-y^2} \leftrightarrow d_{xy}$	-0.0147	0.0146	0.0000	0.0053	-0.0048	0.0000

Appendix B. 1NN and 3NN hopping amplitudes in $\text{Na}_3\text{Co}_2\text{SbO}_6$

Hopping	1 st NN			3 rd NN		
	X	Y	Z	X	Y	Z
$d_{z^2} \rightarrow d_{z^2}$	0.0001	-0.0096	-0.0590	0.0060	0.0011	0.0244
$d_{zx} \rightarrow d_{zx}$	-0.1478	0.0390	0.0352	0.0049	0.0073	-0.0010
$d_{yz} \rightarrow d_{yz}$	0.0483	-0.1449	0.0272	0.0055	0.0047	-0.0071
$d_{x^2-y^2} \rightarrow d_{x^2-y^2}$	-0.0624	-0.0463	0.0060	0.0060	0.0206	0.0018
$d_{xy} \rightarrow d_{xy}$	0.0365	0.0365	-0.1312	0.0009	-0.0103	0.0029
$d_{z^2} \leftrightarrow d_{zx}$	-0.0482	0.0074	-0.0219	-0.0124	0.0176	-0.0159
$d_{z^2} \leftrightarrow d_{yz}$	-0.0021	0.0616	0.0220	-0.0158	0.0089	0.0096
$d_{z^2} \leftrightarrow d_{x^2-y^2}$	-0.0167	0.0270	-0.0223	0.0175	-0.0150	0.0016
$d_{z^2} \leftrightarrow d_{xy}$	0.0142	0.0059	-0.1213	-0.0018	0.0016	-0.0167
$d_{zx} \leftrightarrow d_{yz}$	-0.0106	-0.0336	0.0234	0.0059	-0.0019	0.0147
$d_{zx} \leftrightarrow d_{x^2-y^2}$	-0.1229	0.0032	0.0057	-0.0167	-0.0061	0.0134
$d_{zx} \leftrightarrow d_{xy}$	-0.0094	0.0239	-0.0497	0.0030	0.0042	-0.0094
$d_{yz} \leftrightarrow d_{x^2-y^2}$	0.0079	-0.1114	0.0205	-0.0154	-0.0171	0.0134
$d_{yz} \leftrightarrow d_{xy}$	-0.0221	0.0359	0.0529	-0.0423	-0.0026	-0.0060
$d_{x^2-y^2} \leftrightarrow d_{xy}$	0.0066	0.0189	-0.0246	-0.0278	0.0229	0.0013

-
- [1] L. Balents, *Nature* **464**, 199 (2010).
- [2] P. Anderson, *Mater. Res. Bull.* **8**, 153 (1973).
- [3] A. Kitaev, *Ann. Phys.* **321**, 2 (2006), january Special Issue.
- [4] P. W. Anderson, *Science* **235**, 1196 (1987).
- [5] M. R. Norman, *Rev. Mod. Phys.* **88**, 041002 (2016).
- [6] Y. Zhou, K. Kanoda, and T.-K. Ng, *Rev. Mod. Phys.* **89**, 025003 (2017).
- [7] S. M. Winter, A. A. Tsirlin, M. Daghofer, J. van den Brink, Y. Singh, P. Gegenwart, and R. Valentí, *J. Phys.: Condens. Matter* **29**, 493002 (2017).
- [8] H. Takagi, T. Takayama, G. Jackeli, G. Khaliullin, and S. E. Nagler, *Nat. Rev. Phys.* **1**, 264 (2019).
- [9] G. Jackeli and G. Khaliullin, *Phys. Rev. Lett.* **102**, 017205 (2009).
- [10] H. Liu and G. Khaliullin, *Phys. Rev. B* **97**, 014407 (2018).
- [11] R. Sano, Y. Kato, and Y. Motome, *Phys. Rev. B* **97**, 014408 (2018).
- [12] M. Songvilay, J. Robert, S. Petit, J. A. Rodriguez-Rivera, W. D. Ratcliff, F. Damay, V. Balédent, M. Jiménez-Ruiz, P. Lejay, E. Pachoud, A. Hadj-Azzem, V. Simonet, and C. Stock, *Phys. Rev. B* **102**, 224429 (2020).
- [13] H. Liu, J. c. v. Chaloupka, and G. Khaliullin, *Phys. Rev. Lett.* **125**, 047201 (2020).
- [14] L. Viciu, Q. Huang, E. Morosan, H. Zandbergen, N. Greenbaum, T. McQueen, and R. Cava, *J. Solid State Chem.* **180**, 1060 (2007).
- [15] W. Chen, X. Li, Z. Hu, Z. Hu, L. Yue, R. Sutarto, F. He, K. Iida, K. Kamazawa, W. Yu, X. Lin, and Y. Li, *Phys. Rev. B* **103**, L180404 (2021).
- [16] K. W. Plumb, J. P. Clancy, L. J. Sandilands, V. V. Shankar, Y. F. Hu, K. S. Burch, H.-Y. Kee, and Y.-J. Kim, *Phys. Rev. B* **90**, 041112 (2014).
- [17] R. D. Johnson, S. C. Williams, A. A. Haghighirad, J. Singleton, V. Zapf, P. Manuel, I. I. Mazin, Y. Li, H. O. Jeschke, R. Valentí, and R. Coldea, *Phys. Rev. B* **92**, 235119 (2015).
- [18] A. Banerjee, C. A. Bridges, J.-Q. Yan, A. A. Aczel, L. Li, M. B. Stone, G. E. Granroth, M. D. Lumsden, Y. Yiu, J. Knolle, S. Bhattacharjee, D. L. Kovrizhin, R. Moessner, D. A. Tennant, D. G. Mandrus, and S. E. Nagler, *Nat. Mat.* **15**, 733 (2016).
- [19] J. c. v. Chaloupka, G. Jackeli, and G. Khaliullin, *Phys. Rev. Lett.* **105**, 027204 (2010).
- [20] Y. Singh, S. Manni, J. Reuther, T. Berlijn, R. Thomale, W. Ku, S. Trebst, and P. Gegenwart, *Phys. Rev. Lett.* **108**, 127203 (2012).
- [21] Y. Singh and P. Gegenwart, *Phys. Rev. B* **82**, 064412 (2010).
- [22] S. K. Choi, R. Coldea, A. N. Kolmogorov, T. Lancaster, I. I. Mazin, S. J. Blundell, P. G. Radaelli, Y. Singh, P. Gegenwart, K. R. Choi, S.-W. Cheong, P. J. Baker, C. Stock, and J. Taylor, *Phys. Rev. Lett.* **108**, 127204 (2012).
- [23] A. Biffin, R. D. Johnson, S. Choi, F. Freund, S. Manni, A. Bombardi, P. Manuel, P. Gegenwart, and R. Coldea, *Phys. Rev. B* **90**, 205116 (2014).
- [24] A. Biffin, R. D. Johnson, I. Kimchi, R. Morris, A. Bombardi, J. G. Analytis, A. Vishwanath, and R. Coldea, *Phys. Rev. Lett.* **113**, 197201 (2014).
- [25] J. G. Rau, E. K.-H. Lee, and H.-Y. Kee, *Phys. Rev. Lett.* **112**, 077204 (2014).
- [26] S. Nishimoto, V. M. Katukuri, V. Yushankhai, H. Stoll, U. K. Röbler, L. Hozoi, I. Rousochatzakis, and J. van den Brink, *Nat. Commun.* **7**, 10273 (2016).
- [27] V. M. Katukuri, S. Nishimoto, V. Yushankhai, A. Stoyanova, H. Kandpal, S. Choi, R. Coldea, I. Rousochatzakis, L. Hozoi, and J. van den Brink, *New J. Phys.* **16**, 013056 (2014).
- [28] Y. Sizyuk, C. Price, P. Wölffe, and N. B. Perkins, *Phys. Rev. B* **90**, 155126 (2014).
- [29] J. c. v. Chaloupka and G. Khaliullin, *Phys. Rev. B* **92**, 024413 (2015).
- [30] I. Kimchi, R. Coldea, and A. Vishwanath, *Phys. Rev. B* **91**, 245134 (2015).
- [31] I. Kimchi and Y.-Z. You, *Phys. Rev. B* **84**, 180407 (2011).
- [32] J. Reuther, R. Thomale, and S. Rachel, *Phys. Rev. B* **90**, 100405 (2014).

- [33] Y. Yamaji, Y. Nomura, M. Kurita, R. Arita, and M. Imada, *Phys. Rev. Lett.* **113**, 107201 (2014).
- [34] K. Foyevtsova, H. O. Jeschke, I. I. Mazin, D. I. Khomskii, and R. Valentí, *Phys. Rev. B* **88**, 035107 (2013).
- [35] S. M. Winter, Y. Li, H. O. Jeschke, and R. Valentí, *Phys. Rev. B* **93**, 214431 (2016).
- [36] W. Wang, Z.-Y. Dong, S.-L. Yu, and J.-X. Li, *Phys. Rev. B* **96**, 115103 (2017).
- [37] Y. S. Hou, H. J. Xiang, and X. G. Gong, *Phys. Rev. B* **96**, 054410 (2017).
- [38] G. Xiao, Z. Xia, W. Zhang, X. Yue, S. Huang, X. Zhang, F. Yang, Y. Song, M. Wei, H. Deng, and D. Jiang, *Cryst. Growth Des.* **19**, 2658 (2019).
- [39] E. Lefrançois, M. Songvilay, J. Robert, G. Nataf, E. Jordan, L. Chaix, C. V. Colin, P. Lejay, A. Hadj-Azzem, R. Ballou, and V. Simonet, *Phys. Rev. B* **94**, 214416 (2016).
- [40] A. K. Bera, S. M. Yusuf, A. Kumar, and C. Ritter, *Phys. Rev. B* **95**, 094424 (2017).
- [41] J. P. Perdew, K. Burke, and M. Ernzerhof, *Phys. Rev. Lett.* **77**, 3865 (1996).
- [42] G. Kresse and J. Furthmüller, *Phys. Rev. B* **54**, 11169 (1996).
- [43] G. Kresse and D. Joubert, *Phys. Rev. B* **59**, 1758 (1999).
- [44] P. E. Blöchl, *Phys. Rev. B* **50**, 17953 (1994).
- [45] S. L. Dudarev, G. A. Botton, S. Y. Savrasov, C. J. Humphreys, and A. P. Sutton, *Phys. Rev. B* **57**, 1505 (1998).
- [46] M. Ångqvist, W. A. Muñoz, J. M. Rahm, E. Fransson, C. Durniak, P. Rozyczko, T. H. Rod, and P. Erhart, *Adv. Theory Simul* **2**, 1900015 (2019).
- [47] A. A. Mostofi, J. R. Yates, Y.-S. Lee, I. Souza, D. Vanderbilt, and N. Marzari, *Comput. Phys. Commun.* **178**, 685 (2008).
- [48] B. H. Kim, G. Khaliullin, and B. I. Min, *Phys. Rev. B* **89**, 081109 (2014).
- [49] K. Foyevtsova, H. O. Jeschke, I. I. Mazin, D. I. Khomskii, and R. Valentí, *Phys. Rev. B* **88**, 035107 (2013).
- [50] G. W. Pratt and R. Coelho, *Phys. Rev.* **116**, 281 (1959).
- [51] S. Toth and B. Lake, *J. Phys.: Condens. Matter* **27**, 166002 (2015).
- [52] S. Das, S. Voleti, T. Saha-Dasgupta, and A. Paramakanti, *Phys. Rev. B* **104**, 134425 (2021).
- [53] S. I. Csiszar, M. W. Haverkort, Z. Hu, A. Tanaka, H. H. Hsieh, H.-J. Lin, C. T. Chen, T. Hibma, and L. H. Tjeng, *Phys. Rev. Lett.* **95**, 187205 (2005).
- [54] S.-H. Baek, S.-H. Do, K.-Y. Choi, Y. S. Kwon, A. U. B. Wolter, S. Nishimoto, J. van den Brink, and B. Büchner, *Phys. Rev. Lett.* **119**, 037201 (2017).